Role of sunlight and oxygen on the performance of photo-Fenton process at near neutral pH using organic fertilizers as iron chelates

N. López-Vinent [a]*, A. Cruz-Alcalde [ab], C. Lai [a], J. Giménez [a], S. Esplugas [a], C. Sans [a]

[a] *Department of Chemical Engineering and Analytical Chemistry, Faculty of Chemistry, University of Barcelona, C/Martí i Franqués 1, 08028 - Barcelona, Spain. Tel: +34934021293. Fax: +34934021291*

[b] *Institute of Environmental Assessment and Water Research – Spanish National Research Council (IDAEA-CSIC), C/Jordi Girona 18-26, 08034 – Barcelona, Spain. Tel: +34934006100 (ext. 5203).*

*Corresponding Author: nuria.lopez@ub.edu

ABSTRACT

Nowadays, reaction mechanisms of photo-Fenton process with chelated iron are not yet clearly defined. In this study, five organic fertilizers were used as iron complexes to investigate the role of sunlight and oxygen in photo-Fenton at near neutral pH. UV absorbance and stability constant of each selected iron chelate is different, and this work demonstrates that these parameters affect the reaction mechanisms in SMX degradation. Irradiation experiments without H_2O_2 revealed that only EDDS-Fe and DTPA-Fe achieved SMX degradation, but different iron release. These results, together with soluble oxygen free experiments, allowed the proposal of complementary reaction mechanisms to those of the classical photo-Fenton. The proposed mechanisms start through the potential photoexcitation of the iron complex, followed by subsequent oxygen-mediated hydroxyl radical generation reactions that are different for EDDS-Fe and DTPA-Fe. Moreover, irradiation experiments using EDTA-Fe and HEDTA-Fe had negligible SMX

degradation despite iron release was observed, evidencing the differences between iron chelates.

KEYWORDS

Photochemistry, Iron complexes, Organic fertilizers, Reactive Oxygen Species, Photoexcitation

1. Introduction

According to UNESCO, around 70% of the total consumed freshwater (up to 90% in some developing countries) is destined to agriculture (FAO, 2021). In front of a water scarcity scenario, reusing wastewater (WW) for agricultural purposes might be a good strategy to reduce the freshwater consumption. Nevertheless, the treated wastewater must accomplish some minimum quality requirements to be reused in crop irrigation. These parameters (like biochemical oxygen demand (BOD_5), *E. coli* and turbidity) are established in a Proposal for a Regulation of the European Parliament and of the Council on minimum requirements for water reuse (Regulation 2020/741/EU).

In the last decades, homogeneous Advanced Oxidation Processes (AOPs) have demonstrated their efficiency in the removal of contaminants of emerging concern and bacterial inactivation (Cruz-Alcalde et al. 2017; Huber et al., 2003; Aguas et al., 2017; López et al., 2017). Among AOPs, photo-Fenton process is a promising technology to remove persistent micropollutants (MPs) (Miralles-Cuevas et al., 2017; Rodríguez-Chueca et al., 2015; López-Vinent et al., 2020a; Serra-Clusellas et al., 2018; Carra et al., 2015). Furthermore, application of iron-based materials in heterogenous AOPs can play a significant role in a full-scale wastewater treatment (Luo et al., 2021). The possibility of using solar light as irradiation source makes the process more economic by reducing a large part of operating costs. Photo-Fenton runs better at acidic pH, thus implying a

subsequent neutralization of the water treated. However, the possibility of working at neutral pH exists, making the process more attractive for full-scale application (De la Obra et al., 2017). Recent studies are focused on the performance of photo-Fenton process at neutral pH using organic fertilizers as an iron source to treat wastewater and reuse it for agricultural purposes (López-Vinent et al., 2020b; López-Vinent et al., 2021; Nahim-Grandos et al., 2019). Organic fertilizers are widely used in agriculture as iron chelates, increasing the bioavailability of iron for crops, preventing iron chlorosis, and avoiding the plant disease, since iron is an essential micronutrient for plant growth (Schenkeveld & Temminghoff, 2011). Thus, wastewaters treated by photo-Fenton with organic fertilizers as iron chelates could be directly applied in soils without the need of chelates removal. However, organic fertilizers applied to agriculture may not be completely absorbed by the plants and therefore may appear in surface or groundwater. So far, their reactivity in the aquatic environment has not been deeply studied. In the literature, there is evidence of the iron chelates reactivity with UV (ultraviolet) radiation and dissolved oxygen, and how these processes could potentially lead to the generation of reactive oxygen species (ROS) (Huang et al., 2012; Clarizia et al., 2017; Miralles-Cuevas et el., 2014; Ahile et al., 2020). These reactions and the photoredox cycle of iron (III) complexes may be important to the environment, contributing for instance to the self-depuration of the aquatic compartments by oxidation of some persistent organic pollutants (Graça et al., 2017; Ciésla et al., 2004).

The mechanisms of photo-Fenton with chelated iron are not yet clearly defined. Both UV absorbance and complex stability vary for the different chelating agents, and therefore the reactions involving radiation and free iron could be also distinct. In particular, organic fertilizers such as DTPA-Fe, HEDTA-Fe and EDDHA-Fe have not yet been studied in this regard. Their stability constants with iron are very different compared to EDDS-Fe,

which is the most investigated iron complex (López-Vinent et al., 2021). Despite this, some authors use the mechanistic knowledge obtained for the EDDS-Fe chelate in a general way, making it extensive to any polycarboxylic acid ligand (L). In the case of photo-Fenton using EDDS-Fe, there is evidence of additional mechanisms to produce hydroxyl radicals ($HO^{\bullet}$) apart from classical photo-Fenton reactions. According to the literature (Stasicka, 2011; Li et al., 2010; Ahile et al., 2020), the photoexcitation of EDDS-Fe leads to the generation of EDDS radical (EDDS$^{\bullet}$) expressed as $L^{\bullet}$ in reaction r1. According to this scheme, the complexes chelated with Fe(III) under irradiation could generate both Fe(II) and ligand-free radical ($L^{\bullet}$) by ligand-to-metal charge transfer (LMCT). Superoxide radical ($O_2^{\bullet-}$) could be formed by the reaction between dissolved oxygen and $L^{\bullet}$ (see r2). Meanwhile, $O_2^{\bullet-}$ and its conjugated acid form could generate hydrogen peroxide (H_2O_2) via r3-7 reactions. Finally, $HO^{\bullet}$ is generated by the Fenton reaction thanks to the available dissolved iron (r9). However, the pH is an important factor to consider given that, at neutral pH, reactions r3, r5, r6 and r7 would take place slower than under acidic conditions, influencing the amount of H_2O_2 formed and consequently the quantity of $HO^{\bullet}$ available to react. In addition, at pH values higher than 4 the concentration of both dissolved iron and photoactive $FeOH^{2+}$ decreases, forming precipitated iron hydroxides and thus affecting reactions r4, r5 and r8.

$$Fe(III) - L + h\nu \rightarrow [Fe(III) - L]^{*} \rightarrow Fe(II) + L^{\bullet} \quad \text{(r1)}$$

$$L^{\bullet} + O_2 \rightarrow O_2^{\bullet-} + L' \quad \text{(r2)}$$

$$O_2^{\bullet-} + H^{+} \leftrightarrow HO_2^{\bullet}\,; \quad p\text{Ka}= 4.8 \quad \text{(r3)}$$

$$Fe(II) + O_2^{\bullet-} + 2H_2O \rightarrow Fe(III) + H_2O_2 + 2OH^{-} \quad \text{(r4)}$$

$$Fe(II) + HO_2^{\bullet} + H_2O \rightarrow Fe(III) + H_2O_2 + OH^{-} \quad \text{(r5)}$$

$$O_2^{\bullet-} + HO_2^{\bullet} + H_2O \rightarrow H_2O_2 + O_2 + OH^{-} \quad \text{(r6)}$$

98 $HO_2^{\bullet} + HO_2^{\bullet} \rightarrow H_2O_2 + O_2$ (r7)

99 $Fe(II) + H_2O_2 \rightarrow Fe(III) + HO^{\bullet} + OH^-$ (r8)

100 The aim of this work is to study the reactivity of some widely used organic fertilizers in
101 the photo-Fenton process under solar radiation and the main involved reaction
102 mechanisms at near neutral pH. Reaction mechanisms of photo-Fenton with different iron
103 complexes are not yet clearly defined. Yet, the mechanistic knowledge obtained for
104 EDDS-Fe (which is the most studied one) is usually employed to generalize the additional
105 reactions in photo-Fenton process at near neutral pH using other iron complexes. In this
106 work, five commercial iron chelates (EDDS, EDTA, DTPA, HEDTA and EDDHA),
107 which are approved by the European Commission for agricultural use (Regulation (EC)
108 No 2003/2003), were selected to investigate the differences in the $HO^{\bullet}$ generation since
109 they present different UV absorbances and stability constants with iron. This fact has
110 helped to investigate the contribution of these parameters on the reaction mechanisms.
111 This includes mechanisms about ROS formation because of the interactions between
112 these compounds and both sunlight and dissolved oxygen in aquatic systems.
113 Sulfamethoxazole (SMX) was chosen as a target compound due to their widespread
114 occurrence in aquatic systems (Golovko et al., 2021; Chen et al., 2021; Bunting et al.,
115 2021; Luo et al., 2014).

116 **2. Material and methods**

117 *2.1. Chemicals*

118 Sulfamethoxazole (SMX), diethylene triamine pentaacetic acid (DTPA, 99%), hydrogen
119 peroxide (H_2O_2) (30% *w/w*), *tert*-butyl alcohol (tBuOH), catalase from bovine liver and
120 EDDS-Na (35% in H_2O) were purchased from Sigma-Aldrich (USA). DTPA-Fe (7% of
121 chelated iron), EDTA-Fe (13.3% of chelated iron) and HEDTA-Fe (13.0% of chelated

iron) were bought from Phygenera (Germany). EDDHA-Fe (6.0% of chelated iron) was acquired from Fertiberia (Spain). All commercial organic fertilizers were 100% pure. Acetonitrile, orthophosphoric acid, sodium bicarbonate ($NaHCO_3$) and iron sulphate heptahydrate ($FeSO_4$ $7H_2O$) were obtained from Panreac Quimica (Spain). Nitrogen gas (N_2 > 99.995) was supplied by Abelló Linde (Spain).

2.2. Experimental set-up and procedure

A Solar simulator (Xenonterm-1500RF.CCI) with a Xenon lamp (1.5 kW) equipped with a UV filter, cutting off wavelengths under 290 nm, was employed to perform all experiments. The apparatus contains a tubular photoreactor (25 cm length x 2 cm diameter) located in the axis of a parabolic mirror made of reflective aluminum, at the bottom of the simulation chamber. An external stirred tank (1 L) was used as a reservoir. During the experiments, the solution from the reservoir tank was continuously pumped (peristaltic pump Ecoline VC-280) to the tubular photoreactor and recirculated back to the reservoir. O-nitrobenzaldeyde actinometry (De la Cruz et al., 2013) was carried out to evaluate the average intensity of incident light (wavelength range: 290-400 nm), obtaining a value of 6.6 x 10^{-7} Einstein s^{-1} (13.9 W m^{-2}). Temperature was kept constant at 25ºC by means of a Haake C-40 cooling bath. A scheme of the irradiation setup can be found elsewhere (López-Vinent et al., 2020a).

For solutions preparation, 1.64 mM of HCO_3^- (calculated in order to represent a relative contribution to $HO^\bullet$ scavenging of less than 3%) was added to ultrapure water to keep pH constant at 7.5±0.2. An appropriate amount of each organic fertilizer chelated with iron was added to achieve a value of 5 mg L^{-1} of iron (maximum allowed concentration for irrigation water) (Guidelines for water reuse 600/r-12/618; Ayers & Westcot, 1985), considering the percentage of iron in each organic fertilizer presented in section 2.1. As EDDS-Fe was not found as a commercial product, it was prepared by mixing EDDS and

147 iron (II) at a molar ratio of 1:1 (EDDS-Fe(II)) (López-Vinent et al., 2021). In that especial
148 case, iron (5 mg L^{-1}) was added to the stirred EDDS solution to guarantee a complete
149 chelation. More details about the experimental procedure of chelation can found
150 elsewhere (López-Vinent et al., 2021). Then SMX, used as a model target compound, was
151 spiked to ultrapure water to have a final concentration of 1 mg L^{-1}. Finally, hydrogen
152 peroxide (concentration of 50 mg L^{-1}) was appended just before turning on the solar
153 simulator. The contribution of dissolved oxygen on the process was evaluated through
154 experiments in which N_2 gas was bubbled during 30 minutes before starting the
155 experiment and throughout the whole reaction time. WTW Oxi 340i Oximeter was used
156 during the test to measure the O_2 concentration. A concentration of 25 mM of tBuOH
157 (contributing to 95% of $HO^{\bullet}$ scavenging) was used to study the role of hydroxyl radical
158 in photo-Fenton experiments with and without H_2O_2. All experiments were performed in
159 duplicate and error bars are shown in the plots.

160 For different analyses, samples were withdrawn from the feeding tank throughout the
161 entire reaction time and catalase (200 mg L^{-1}) was employed to quench the residual H_2O_2.
162 When iron in solution was determined, the samples were filtered with 0.20 μm PVDF
163 filter to analyze only the dissolved iron. Then, excess of ascorbic acid was added to obtain
164 total soluble iron.

165 The accumulated energy (Q_{acc}, kJ L^{-1}) was calculated according to Eq.1 (Romero Olarte,
166 2015).

167 $$Q_{acc} = \sum_{i=1}^{n} \frac{I \cdot \Delta t_i}{V} \quad \text{(Eq.1)}$$

168 where I corresponds to the average intensity of incident light (kJ s^{-1}), Δt_i is the increment
169 of the reaction' time (s) and V is the volume (L).

170 *2.3. Analytical methods*

SMX concentrations were determined by High Performance Liquid Chromatography (HPLC) with UV detection (1260 Infinity Series from Agilent). Acetonitrile and orthophosphoric water solution acidified at pH=3 (60:40 volumetric mixture, respectively) were employed as mobile phases. An isocratic method at 1 mL min^{-1} and 100 µL of volume injection were selected. The column used was a Tecknokroma Mediterrania Sea C-18 (250 x 4.6 mm i.d, 5µm particle size), and the UV detector was set at 270 nm. For the determination of hydrogen peroxide, a colorimetric method based on the use of metavanadate was employed (Pupo Nogueira et al., 2005). A procedure based on o-phenatroline (ISO 6332) was employed to measure the total dissolved iron. Absorbance spectra were recorded by using a UV-Vis spectrophotometer DR6000 by Hach (USA).

3. Results and discussion

The photodegradation of three new iron chelates (DTPA-Fe, HEDTA-Fe and EDDHA-Fe) was studied over a long period of time to emphasize the importance of the iron chelates stability. EDDS-Fe and EDTA-Fe were also investigated for comparison purposes.

The absorption spectra of iron chelates were obtained in ultrapure water and it was used to evaluate the possibility of iron complexes undergoing photodegradation (Figure 1). The UV light absorption band in all these compounds overlap to the emission spectrum of the solar simulator (290-600 nm), as shown in Figure 1. This depicts the capacity of these iron complexes to absorb radiation at the UVA and UVB range.

Figure 1. UV-Vis absorption spectrum of five iron chelates (EDDS-Fe, EDTA-Fe, DTPA-Fe, HEDTA-Fe and EDDHA-Fe) at 5 mg L^{-1} of iron.

196 *3.1. Contribution of solar simulated radiation*

197 *3.1.1. Photo-Fenton and dark Fenton experiments*

198 To elucidate the contribution of simulated solar radiation on SMX abatement when the
199 five iron chelates (EDDS-Fe, EDTA-Fe, DTPA-Fe, HEDTA-Fe and EDDHA-Fe) were
200 used in photo-Fenton at pH=7.5 ± 0.2, photo-Fenton tests (chelate-Fe + H_2O_2 + sunlight)
201 together with Fenton reaction (chelate-Fe + H_2O_2) and experiments without H_2O_2
202 (chelate-Fe + sunlight) were performed. The SMX depletion results are shown in Figures
203 2a,3a and 4a respectively. The evolution of total iron corresponding to each experiment
204 is displayed in Figures 2b, 3b and 4b. The plots present results for 1.5 kJ L^{-1},
205 corresponding to 2h of experiment. Blank tests were also carried out to clarify the
206 potential mechanisms for SMX degradation. No removal was observed in the photolysis
207 experiment. In addition, H_2O_2 combined with radiation led to a value of 9.7% of SMX
208 abatement, this caused by H_2O_2 decomposition by light giving place to two hydroxyl
209 radical molecules (see reaction r9). However, in photo-Fenton experiments this
210 contribution was probably lower due to the strong "inner filter effect" caused by the
211 absorption of light by Fe-complexes (Pignatello et al., 2006).

212 $H_2O_2 + h\nu \rightarrow 2\,HO^{\cdot}$ (254-299 nm) (r9)

213

214 **Figure 2.** a) SMX abatement and b) evolution of total dissolved iron plotted as a function of the accumulated energy
215 for photo-Fenton experiments with five different iron chelates at pH = 7.5. The pH during entire experiments was kept
216 constant at 7.5 ± 0.2. $[SMX]_0$ = 1 mg L^{-1}; $[Fe]_0$ = 5 mg L^{-1}; $[H_2O_2]_0$ = 50 mg L^{-1}.

217

218 From Figure 2a, different behaviour concerning SMX degradation can be appreciated in
219 photo-Fenton at near neutral pH, depending on the iron chelate that was employed as iron
220 source. Total SMX removal was achieved at the end of the treatment when using EDTA-

221 Fe (1.5 kJ L^{-1}; 120 min) while in the case of EDDHA-Fe only a 17.8% of degradation
222 was observed. Experiments with EDDS-Fe showed the highest degradation kinetics until
223 0.6 kJ L^{-1} (corresponding to 45 min), then dropped significantly until nearly complete
224 degradation (93.3% at 1.5 kJ L^{-1}). DTPA-Fe and HEDTA-Fe mediated treatments resulted
225 in close removal profiles throughout the entire experiment, obtaining a degradation of
226 91.0 and 90.2% at 1.5 kJ L^{-1}, respectively. As mentioned before, the ligand properties are
227 important in reactions involving iron chelates. In this sense, the stability constant of each
228 ligand with iron is an important parameter to be considered, but not the only one. Highest
229 stability constant value amongst the studied chelates is 35.1, corresponding to EDDHA-
230 Fe(III) (Sierra et al., 2004). This value is in accordance with the lowest total iron
231 precipitation (3.6% at the end of the experiment) observed through experimentation (see
232 Figure 2b), and also with the lowest SMX degradation (see Fig. 2a). On the contrary,
233 EDDS showed the highest precipitation of iron (71.2% at 1.5 kJ L^{-1}), in accordance with
234 its stability constant value with iron (III), that is, 22.0 (Orama et al., 2002). The stability
235 constants with iron (III) for EDTA, DTPA and HEDTA are 25.1, 28.6 (Dojindo Molecular
236 Technologies, 2020) and 19.8 (Martell et al., 1996), respectively, and the iron
237 precipitation at the end of the experiment was 37.4%, 8.1% and 7.7%, respectively (see
238 Figure 2b). From these results it seems that a high ligand-Fe stability constant acts
239 reducing the SMX degradation. However, a clear trend in this way was not observed. For
240 instance, even though HEDTA and DTPA have different stability constants of their
241 complexes with iron (III), both iron precipitation and SMX removal were very similar.
242 This fact could evidence the existence of other structural factors of iron chelates that could
243 affect to hydroxyl radical generation mechanisms, apart from the classical Fenton and
244 photo-Fenton reactions.

In the literature related to the Fenton reactions with EDDS-Fe chelates, some authors state that reactions between oxidants and EDDS-Fe complexes could be interpreted analogously to homogeneous processes taking place with free iron under acidic medium conditions (reaction r10 and r11) (Huang et al., 2013). Other works suggest an additional contribution to pollutants degradation via the breakdown of Fe-EDDS complex in Fenton reactions, forming EDDS radical (EDDS$^{\bullet}$) (reaction r12 and r13) (Miralles-Cuevas et al., 2019) or EDDS$^{\bullet+}$ (reaction r14) (Wu et al., 2014) together with radical species like hydroxyl and superoxide radicals.

$$Fe(II) - EDDS + H_2O_2 \rightarrow Fe(III) - EDDS + HO^{\bullet} + OH^{-} \quad \text{(r10)}$$

$$Fe(III) - EDDS + H_2O_2 \rightarrow Fe(II) - EDDS + HO_2^{\bullet}/O_2^{\bullet-} + H^{+} \quad \text{(r11)}$$

$$Fe(II) - EDDS + H_2O_2 \rightarrow Fe(III) + EDDS^{\bullet} + HO^{\bullet} + OH^{-} \quad \text{(r12)}$$

$$Fe(III) - EDDS + 2\,H_2O_2 \rightarrow Fe(II) + EDDS^{\bullet} + O_2^{\bullet-} + 2\,OH^{-} \quad \text{(r13)}$$

$$Fe(III) - EDDS + H_2O_2 \rightarrow Fe(II) + EDDS^{\bullet+} + HO_2^{\bullet}/O_2^{\bullet-} + H^{+} \quad \text{(r14)}$$

To determine the possible contribution of iron chelate breakdown to the Fenton performance when using the studied fertilizers, experiments under dark conditions were performed (see Figure 3a). The evolution of total iron was also evaluated and displayed in Figure 3b. EDDHA-Fe was not included due to the low degradation in Fenton tests at the end of the treatment.

Figure 3. a) SMX abatement and b) evolution of total dissolved iron plotted as a function of the accumulated energy for Fenton experiments with four different iron chelates at pH = 7.5. The pH during entire experiments was kept constant at 7.5 ± 0.2. [$[SMX]_0$ = 1 mg L^{-1}; $[Fe]_0$ = 5 mg L^{-1}; $[H_2O_2]_0$ = 50 mg L^{-1}.

From the iron precipitation displayed in Fig. 3b, it was deduced that the main reactions in Fenton process when using DTPA-Fe, HEDTA-Fe and EDTA-Fe are reaction r10 and r11, since the ligand-Fe breakdown and iron release is minimum. In the case of EDDS-Fe, the iron precipitation was significantly higher, up to 28.4% after 2 hours of treatment. Therefore, these results agree with previous works performed with EDDS (reactions r10-13).

Comparing Figures 2a and 3a, the role of solar irradiation in the photo-Fenton experiments can be appreciated. Pseudo-first order kinetics corresponding to Fenton and photo-Fenton experiments are presented in Table 1. In photo-Fenton experiments with EDDS-Fe, a high iron release was observed from 30 minutes of reaction. This fact implies that the kinetics from this point cannot be considered as pseudo-first order, and EDDS-Fe kinetics were determined only until 30 minutes. The kinetics of EDDS-Fe were not compared with the kinetics of other organic fertilizers since in these cases the pseudo-first order kinetics was evaluated until 120 minutes.

Table 1. Removal of SMX and total iron in solution in photo-Fenton and Fenton tests at near neutral pH, with different organic fertilizers. The presented values are at the end of the treatment (1.5 kJ L^{-1}; 120 min). k is the calculated kinetic constant (pseudo-first order) for each ligand-Fe (from 0 to 1.5 kJ L^{-1}, 120 min). *For EDDS, kinetic constants for both treatments were calculated considering data obtained from 0 to 0.39 kJ L^{-1} (30 min), i.e., within the linear range of the pseudo first-order plot.

DTPA-Fe, HEDTA-Fe and EDTA-Fe photo-Fenton tests achieved higher degradations than Fenton experiments at the end of the treatment (see Table 1). This can be related to the existence of a photoredox cycle for iron, which in presence of solar light reduces iron

chelates from Fe(III) to Fe(II), yielding hydroxyl radicals during the process (r15) (*Ligand* applicable to DTPA, HEDTA and EDTA).

$$Fe(III) - Ligand + hv + H_2O \rightarrow Fe(II) - Ligand + HO^{\bullet} + H^{+} \quad \text{(290-600 nm) (r15)}$$

However, there were significant differences in the precipitation of iron in all cases (see Figures 2b, 3b and Table 1). In the presence of solar light, the breakdown of iron complexes may be due to the attack of hydroxyl radical and/or photodegradation, depending on the structure of the ligand. The iron precipitation in experiments performed with DTPA-Fe and HEDTA-Fe was only 2% higher in photo-Fenton, compared to Fenton process. Thus, in those cases, the contribution of irradiation on the breakage of the iron complexes was minimum. This is in agreement with the higher stability of these compounds. For EDTA, iron remained in the form of chelate during Fenton reaction (5% of iron precipitation), but the precipitation of this element reached 37.4% at the end of the photo-Fenton treatment, indicating the contribution of photodegradation to the chelate breakage process. In the case of EDDS-Fe, interestingly, this seems to proceed through both pathways (28.4% and 71.2% of iron precipitation for Fenton and photo-Fenton tests, respectively). In that case, the influence of irradiation together with the possible $HO^{\bullet}$ contribution to iron complex breakage is more evidenced in photo-Fenton. These results are in accordance with the lowest stability constant of the EDDS-iron chelate.

From the results obtained in Fenton and photo-Fenton experiments shown in Table 1, it is also observed that the irradiation effect on SMX degradation is different depending on the stability of iron chelate with iron. The SMX oxidation rates in DTPA-Fe and HEDTA-Fe mediated photo-Fenton were only 2.2 and 2.5 times higher than those in Fenton, respectively, in accordance with their higher stability compared to that of the other chelates. On the other hand, the degradation kinetics were 11 and 8.4 times faster when employing less stable EDTA-Fe and EDDS-Fe complexes. However, the latter

317 represented a special case. Even though at the initial reaction times (corresponding up to
318 0.39 kJ L^{-1}) SMX degradation rate was the highest, it reached the lowest degradation
319 percentage at the end of the treatment (only 47.5%). This fact could be related to the r10
320 reaction where the Fe(II)-EDDS reacts with H_2O_2, consequently yielding a great
321 production of hydroxyl radicals due to the low stability of that chelating agent with iron.

322 In summary, and according with 0 results and those from the literature, there are strong
323 evidences of photoexcitation of EDDS-Fe and subsequent potential formation of EDDS
324 radical (EDDS$^{\bullet}$), which can be involved in further reactions to generate hydroxyl radicals.
325 In that case, the precipitation of iron was very high. However, the precipitation of iron
326 when applying the other organic fertilizers was significantly lower. These data, together
327 with the comparison between Fenton and photo-Fenton experiments, point out that the
328 generated species and mechanisms participating in the solar photo-Fenton process could
329 be different for each chelating agent.

330 *3.1.2. Irradiation experiments without H_2O_2*

331 Irradiation experiments without H_2O_2 were carried out with the different iron chelates
332 (see Figures 4a, 4b) to establish the relative photo-susceptibilities of the different
333 complexes and its influence on the degradation mechanisms of target MPs.

334

335 **Figure 4.** a) SMX abatement and b) evolution of total dissolved iron plotted as a function of the accumulated energy
336 for irradiation experiments without H_2O_2 for five different iron chelates at pH = 7.5. The pH during entire experiments
337 was kept constant at 7.5 ± 0.2. $[SMX]_0$ = 1 mg L^{-1}; $[Fe]_0$ = 5 mg L^{-1}.

338

339 As it can be observed in Figure 4a, the irradiation tests with EDDS-Fe and DTPA-Fe
340 yielded significant SMX removal. At the end of the experiment (1.5 kJ L^{-1}; 120 min), the

degradation results were 43.5 and 30.0% for EDDS-Fe and DTPA-Fe, respectively. The result of EDDS-Fe was not fully unexpected, as a similar behavior has been observed in previous studies related to photodegradation of this iron complex (Huang et al., 2012; Ciésla et al., 2004; Li et al., 2010; Huang et al., 2013). In Particular, Ciésla and coworkers (Ciésla et al., 2004) proposed a photodegradation mechanism for EDDS-Fe that lies in the photoreduction of Fe(III) complex induced by light by the ligand-to-metal charge transfer (LMCT) (reaction r16; 290-600 nm). This excitation can lead to a reduction of Fe(III) to Fe(II) followed by one-electron oxidation of the ligand by the inner-sphere photoinduced electron transfer (Ciésla et al., 2004).

$$[Fe(III)-EDDS]^{-} + hv\,(LMCT) \rightarrow [Fe(III)-EDDS]^{*-} \rightarrow Fe(II) + EDDS^{\bullet 3-} \quad \text{(r16)}$$

The radical formed via reaction r16 ($EDDS^{\bullet 3-}$) tends to reach its stable oxidation state requiring a second electron transfer through reaction with dissolved oxygen (reaction r17) (Ciésla et al., 2004).

$$EDDS^{\bullet 3-} + O_2 \rightarrow EDDS^{2-} + O_2^{\bullet -} \quad \text{(r17)}$$

The superoxide radical generated in r17 can take part in additional reactions as a precursor of hydroxyl radical.

Additionally, $EDDS^{\bullet 3-}$ can react with the Fe(III) complex, enhancing the Fe(III)/Fe(II) cycle (reaction r18), as well as with hydroxyl ion (OH^-) to generate $HO^{\bullet}$ (reaction r19).

$$[Fe(III)-EDDS]^{-} + EDDS^{\bullet 3-} \rightarrow [Fe(II)-EDDS]^{2-} + EDDS^{2-} \quad \text{(r18)}$$

$$EDDS^{\bullet 3-} + HO^{-} \rightarrow EDDS^{4-} + HO^{\bullet} \quad \text{(r19)}$$

According to our data, gathered in Figures 4a and b, the results of experiments employing EDDS-Fe appear to indicate the possibility of generating $EDDS^{\bullet 3-}$ due to the photodegradation of Fe-complex, causing the release of a great amount of Fe (II) during the process. This is supported by the experimental observation that a large part of the iron

precipitates. However, a small part of the metal could react with superoxide radical to generate H_2O_2 (reaction r20) (Li et al., 2010). On its part, $[Fe(II)\text{-}EDDS]^{2-}$ formed in reaction (r18) can also react with superoxide radical to produce H_2O_2 (reaction r21).

$$Fe(II) + O_2^{\bullet -} + 2H_2O \rightarrow Fe(III) + H_2O_2 + 2HO^- \quad \text{(r20)}$$

$$[Fe(II) - EDDS]^{2-} + O_2^{\bullet -} + 2H_2O \rightarrow [Fe(III) - EDDS]^- + H_2O_2 + 2HO^- \quad \text{(r21)}$$

As observed in Figures 4a and b, not all Fe-complexes had the same behavior as that observed for EDDS-Fe. DTPA-Fe irradiation experiments resulted in 30.0% of SMX abatement but only 8.0% iron precipitation and, consequently, the reduction of Fe(III) to Fe(II) from the photoexcitation of the complex and subsequent iron complex breakage (reaction r22) did not occur significantly. Thus, the main photo-induced reactions mechanism for oxidants generation with DTPA-Fe would be different from those of EDDS-Fe. The main involved reactions are proposed for first time in this study and presented in r23 and r24.

$$[Fe(III) - DTPA]^- + h\nu\ (LMCT) \rightarrow [Fe(III) - DTPA]^{*-} \rightarrow Fe(II) + DTPA^{\bullet 3-} \quad \text{(290-600 nm) (r22)}$$

$$[Fe(III) - DTPA]^{*-} + O_2 \rightarrow [Fe(III) - DTPA^{\bullet 3-}] + O_2^{\bullet -} \quad \text{(r23)}$$

$$[Fe(III) - DTPA^{\bullet 3-}] + HO^- \rightarrow [Fe(III) - DTPA]^- + HO^{\bullet} \quad \text{(r24)}$$

In the case of DTPA, the electron transfer to molecular oxygen would proceed through the excited Fe(III)-complex ($[Fe(III)\text{-}DTPA]^{*-}$] to generate superoxide radical (reaction r23), which would be involved in further reactions to generate hydroxyl radical. However, the reduction of $[Fe(III)\text{-}DTPA]^-$ to $[Fe(II)\text{-}DTPA]^{2-}$ and subsequent formation of H_2O_2 are possible by reactions (r15) and (r21), respectively. In addition, H_2O_2 could also be generated by reaction (r20), even though this is unlikely as only 8.0% of iron release was observed in the tests conducted with this organic fertilizer.

388 Further experiments without H_2O_2 were performed to investigate the possible formation
389 of H_2O_2 by means of irradiation (290-600 nm) of DTPA-Fe solutions. The results
390 suggested the generation of small amounts of H_2O_2, with maximum observed
391 concentrations of 0.7 mg L^{-1} after two hours of experiment. By increasing iron
392 concentration (in the form of DTPA-iron chelates) to 20 mg L^{-1}, which also implies an
393 increase of the ligand concentration, the maximum detected concentration of H_2O_2 was
394 5.2 mg L^{-1}. Thus, in the experiments without initial H_2O_2 (Figure 4a), its generation could
395 produce $HO^{\bullet}$ by photo-Fenton reactions, a fact which agreed with the little consumption
396 of hydrogen peroxide observed during the photo-Fenton experiments (data not shown).
397 Additionally, experiments without iron were performed to ensure that the photoactive
398 species were the Fe-complexes. No SMX degradation was observed, confirming the
399 suggested reactions.

400 EDTA-Fe and HEDTA-Fe displayed a completely different behaviour. In these cases,
401 especially for EDTA-Fe, a photoexcitation of the complex was inferred based on iron
402 precipitation throughout the experiment (30.7% of iron release for EDTA-Fe at 2 hours).
403 This amount is higher than that for DTPA-Fe (only 6.0% at the end of the experiment),
404 but the degradation of SMX was almost null in EDTA-Fe (only 6.3%). In the case of
405 HEDTA-Fe, these values were 15.8% and 6.2% for iron precipitation and SMX removal,
406 respectively. These results suggest that the species formed by the photodegradation of
407 EDTA-Fe and HEDTA-Fe would not be involved in ROS generation in the same way as
408 in the case of EDDS-Fe and DTPA-Fe. For this reason, when degradation mechanisms
409 are evaluated, it is important to study diverse iron complexes, as their different
410 characteristics can lead to different behaviours.

411 To understand the role of superoxide radical probably formed in the above reaction
412 mechanisms, experiments with *tert*-butyl alcohol in the photo-Fenton tests were also

carried out and depicted in Figure 5. EDDHA-Fe was not studied in this regard due to its low SMX degradation in photo-Fenton experiments. tBuOH has an elevated reaction rate with $HO^{\bullet}$ (6 x 10^8 M^{-1} s^{-1}) (Piechowski et al., 1992). Scavengers of superoxide radical, like benzoquinone, were not employed in this study because they are not completely selective for $O_2^{\bullet-}$ (in general they also react with $HO^{\bullet}$) (Bustos et al., 2019). Experiments with other scavengers such as ascorbic acid were not performed since this substance presents a much higher reaction rate with $HO^{\bullet}$ (1.1 x 10^{10} M^{-1} s^{-1}) than with $O_2^{\bullet-}$ (5 x 10^4 M^{-1} s^{-1}) (Shen et al., 2021). Thus, the effect of ascorbic acid on the SMX degradation performance should be similar than employing tert-Butanol. Additionally, since iron (III) also reacts with ascorbate (4.7 x 10^4 M^{-1} s^{-1}), it could interfere with the results (Shen et al., 2021).

Figure 5. SMX degradation as a function of the accumulated energy for photo-Fenton experiments with tBuOH for four different iron chelates at pH=7.5. The pH during entire experiments was kept constant at 7.5 ± 0.2. $[SMX]_0$ = 1 mg L^{-1}; $[Fe]_0$ = 5 mg L^{-1}; $[H_2O_2]$ = 50 mg L^{-1}; [tBuOH] = 25 mM.

As it can be observed in Figure 5, the same level of SMX degradation was reached for all EDTA-Fe, DTPA-Fe and HEDTA-Fe complexes when tBuOH was present in the reaction medium (about 5.0% of SMX removal at the end of the treatment). Only EDDS-Fe achieved the slightly higher value of 9.2% in 2 hours. As tBuOH was calculated to scavenge 95% of available HO•, the results most likely indicated that hydroxyl radical generated directly by photo-Fenton reactions and mediated by the photoexcitation of Fe-complexes (EDDS-Fe and DTPA-Fe) was the specie involved in the degradation of SMX. In the case of EDDS-Fe, however, the observed 9.2% abatement (when tBuOH was added) confirmed that other ROS would be involved in the degradation mechanisms of SMX in the presence of dissolved oxygen.

To complete this section, experiments with non-chelated iron were investigated in an attempt of elucidating the possible involvement of free iron in solution in the SMX degradation mechanisms. This iron is formed from the breakdown of the iron complex and before generating $Fe(OH)_2^+$, which is the predominant specie at pH=7.5 (Pignatello et al., 2006). As observed, when organic fertilizers complexed with iron were used, the greater iron release was followed by a higher reaction rate in SMX. This fact can lead to confusion with regard to the degradation mechanisms. For this reason, the precipitation curves in photo-Fenton experiments catalyzed by EDDS-Fe and DTPA-Fe (Figure 2b) were used to determine the potential free iron in solution for both experiments. From Figure 2b, the difference in concentration of chelated iron in solution at two different times DTPA-Fe and EDDS-Fe (e.g., the concentration of iron precipitated between 0 and 5 min. (i.e., 0 and 0.1 kJ L^{-1}), 5 and 15 min (i.e., 0.1 kJ L^{-1} and 0.2 kJ L^{-1}) …) was used to elaborate a Fe(II) dosing plan during the experiments without chelating agent. The selection of these two organic fertilizers was decided with the objective to study the iron dose at different concentrations, being the highest iron dose with EDDS-Fe and the lowest with DTPA-Fe since EDDS-Fe presented the highest iron release and DTPA-Fe the lowest one in the previous experiments. The dosage plan is depicted in Figures 6a and 6b. Figure 6a corresponds to the iron concentration added at each time (min) or energy (kJ L^{-1}). Thus, the iron concentration added at 0 kJ L^{-1} (0 min) corresponds to the concentration of iron which was precipitated in the photo-Fenton experiments between 0 and 5 minutes (0 and 0.1 kJ L^{-1}). In the same way, the iron concentration added at 0.8 kJ L^{-1} (60 min) corresponds the iron release between 60 and 120 minutes (0.8 and 1.5 kJ L^{-1}). The same applies to the other intervals considered (0.1, 0.2 and 0.4 5 kJ L^{-1}). Figure 6b was referred to the accumulated iron added during the Fe (II) dosage experiment, and not to the total dissolved iron. As the pH was 7.5, part of this added Fe (II) precipitated due to the

formation of $Fe(OH)_2^+$. In Figure 6b it was observed that a total of 2.2 mg L^{-1} of Fe (II) was added in one case, following the precipitation curve of iron in EDDS-Fe (see Figure 2b where 2.2 mg L^{-1} of iron were precipitated at 120 min). Following the iron precipitation curve of DTPA-Fe, only 0.4 mg L^{-1} of Fe (II) precipitated at the end of the experiment, this corresponding to the total iron added in the experiments without chelating agent (Figure 6b). To perform these experiments, a stock solution of Fe (II) at pH=2.8 was prepared. From these stock solution, different aliquots were taken at selected times and added to the solution to be treated. To compare with photo-Fenton experiments with organic fertilizers, the pH of the solution was followed during the entire reaction, remaining constant until the end of the experiment (pH = 7.5 ± 0.2).

Figure 6. a) Iron dosification b) accumulated iron as a function of the accumulated energy in photo-Fenton experiments without chelating agents following the iron precipitation curves of photo-Fenton using EDDS-Fe and DPTA-Fe. pH =7.5. The pH during entire experiments was kept constant at 7.5 ± 0.2. $[SMX]_0$ = 1 mg L^{-1}; $[H_2O_2]$ = 50 mg L^{-1}.

The results of the SMX removal at the end of the experiment (2 hours, 1.5 kJ L^{-1}) were 16.6 and 13.7% for the total dosage of 2.2 and 0.4 mg L^{-1}, respectively, corresponding to the iron precipitation curve of EDDS-Fe and DTPA-Fe. These results represented a great reduction of SMX removal compared to photo-Fenton using organic fertilizers, where 94.7 and 91.0% were respectively reached at 2 hours. This fact evidenced that under the studied conditions, iron chelates were involved in the photo-Fenton reactions. A small part of the SMX degradation could be caused by dissolved iron before precipitating as Fe(III) oxyhydroxides. However, it was not the main generation pathway for $HO^{\bullet}$.

3.2. Contribution of dissolved oxygen

To corroborate the role of dissolved oxygen on photo-Fenton reactions catalyzed by Fe-complexes, photo-Fenton tests were subjected to continuous N_2 bubbling. The results are depicted in Figures 7a, b, c and d, corresponding to experiments with EDDS-Fe, EDTA-Fe, DTPA-Fe and HEDTA-Fe, respectively. In the case of EDDS-Fe and DTPA-Fe, experiments without H_2O_2 were also tested under N_2 bubbling. The results are also shown in Figures 7a and 7c. Table 2 reports the corresponding pseudo-first order reaction rates.

Figure 7. Photo-Fenton experiments without dissolved O_2 (continuously bubbling N_2) for a) EDDS-Fe, b) EDTA-Fe, c) DTPA-Fe and d) HEDTA-Fe as a function of the accumulated energy. Opened symbols corresponds to irradiation experiments without H_2O_2 and closed symbols refers to photo-Fenton experiments. pH =7.5. The pH during entire experiments was kept constant at 7.5 ± 0.2. $[SMX]_0 = 1$ mg L^{-1}; $[H_2O_2] = 50$ mg L^{-1}.

Table 2. Pseudo-first order kinetics and SMX removal for each organic fertilizer in photo-Fenton with and without dissolved O_2 (from 0 to 1.5 kJ L^{-1}, 120 min). *For EDDS, kinetic constants for two treatments were calculated considering data obtained from 0 to 0.39 kJ L^{-1} (30 min), i.e., until a linear trend is observed in the pseudo first-order plot.

From the results presented in Figure 7 and Table 2, it can be observed that dissolved oxygen plays an important role in the SMX degradation mechanisms in all cases. The reductions in kinetic constants in anoxic conditions, compared to photo-Fenton experiments with dissolved oxygen, were: 3.8, 2.7, 2.0 and 2.3 times for EDDS-Fe, EDTA-Fe, DTPA-Fe and HEDTA-Fe, respectively. As the iron release was the same in the two types of experiments, the results suggested that the role of the oxygen was more important at greater iron precipitation (and possible subsequent ligand radical formation). This fact evidenced the reactions described in section 3.1.2 where the Fe-complexes together with irradiation (290-600 nm) could lead the formation of superoxide radical as

514 a precursor of hydroxyl radicals. This fact can also be observed in Figures 7a and 7c,
515 where results of experiments using EDDS-Fe and DTPA-Fe without H_2O_2 nor O_2 were
516 represented. Irradiation experiments without H_2O_2 achieved 43.5% and 30.0% of SMX
517 removal for EDDS-Fe and DTPA-Fe, respectively. However, under anoxic conditions the
518 SMX degradations were reduced to 7.8 and 11.0% for EDDS-Fe and DTPA-Fe,
519 respectively, evidencing the role of oxygen in the removal mechanisms. The low SMX
520 abatement seen in these last experiments could be related to the generation of H_2O_2
521 through reactions explained in section 3.1.2.

522 Finally, in the case of EDTA-Fe and HEDTA-Fe it was seen that the mechanisms could
523 be a little different due to low SMX degradation was observed in the experiments without
524 H_2O_2. Probably in these cases, due to the characteristics of the organic fertilizers, the
525 radical generated could be involved in the Fe(III)/Fe(II) cycle in photo-Fenton process as
526 an additional way to produce hydroxyl radicals (Huang et al., 2012; Pigantello et al.,
527 2006).

528 **4. Conclusions**

529 In photo-Fenton experiments, all iron complexes obtained more than 90% of SMX
530 removal after 2 hours, except EDDHA-Fe, which only achieved a degradation of 17.8%.
531 Moreover, from the comparison of Fenton and photo-Fenton results it was revealed that
532 radiation plays an important role in the photoredox cycle of iron and subsequent hydroxyl
533 radical generation, especially for iron complexes less stable such as EDDS-Fe and EDTA-
534 Fe.

535 Additional mechanisms to generate hydroxyl radicals in irradiation experiments at
536 circumneutral pH with iron complexes have been observed in this study. The five organic
537 fertilizers tested (EDDS-Fe, EDTA-Fe, DTPA-Fe, HEDTA-Fe and EDDHA-Fe) present

538 differences in additional vias to produce $HO^{\bullet}$, due to their different UV absorbance and
539 stability constant of chelate with iron. Although all organic fertilizers absorb in the range
540 of 290-400 nm, only EDDS-Fe and DTPA-Fe showed significant SMX degradation
541 (43.5% and 30.0%, respectively). However, since the iron release was very different (70.0
542 and 8.0% for EDDS-Fe and DTPA-Fe, respectively), the mechanisms in hydroxyl radical
543 formation are potentially different. Since in tests using DTPA-Fe the iron precipitation
544 was minimum, the proposed mechanisms established that the electron transfer to
545 molecular oxygen would proceed through the excited Fe-complex ($[Fe(III)\text{-}DTPA]^{*-}$] to
546 generate the superoxide radical and subsequent hydroxyl radicals generation. However,
547 the photoexcitation of EDDS-Fe complex leads to the breakage of the complex and
548 subsequent formation of EDDS radical ($EDDS^{\bullet 3-}$), which is the specie involved in
549 generation of $HO^{\bullet}$. The experiments performed with EDTA-Fe and HEDTA-Fe
550 evidenced again that photoexcitation mechanisms are different for iron complexes. In
551 those cases, only 6% of SMX degradation was achieved and 30.7 and 15.8% of iron
552 release were observed for EDTA-Fe and HEDTA-Fe, respectively.

553 The scavenging experiments with tBuOH determined that hydroxyl radicals were the final
554 specie responsible to SMX removal. Additionally, the photo-Fenton experiments
555 bubbling N_2 revealed the importance of oxygen-mediated reactions in the in the
556 generation of radicals at neutral pH with iron complexes, being reinforced by the increase
557 in SMX abatement in presence of dissolved oxygen.

558 Finally, photo-Fenton tests with non-chelated iron were done to elucidate the possible
559 involvement of free iron in solution (formed in the breakage of the iron complex and
560 before it precipitates) in the SMX degradation mechanisms. Experiments presented lower
561 SMX removal (16.6% at 2 hours, with higher iron concentration added) than experiments

562 with iron chelates, demonstrating that the photo-Fenton reactions with iron complexes are
563 the main pathway in the process.

564 **Acknowledgments**

565 The authors are grateful with the Ministry of Economy and Competitiveness (project
566 CTQ2017-86466-R, MINECO/FEDER, UE), AGAUR-Generalitat de Catalunya (project
567 2017SGR-131) and Nuria López FPU research fellowship (FPU-16/02101) financed by
568 Ministry of Science, Innovation and Universities.

569 **References**

570 Aguas, Y., Hincapie, M., Fernández-Ibáñez, P., Polo-López, M.I., Solar photocatalytic
571 disinfection of agricultural pathogenic fungi (*Curvularia sp.*) in real urban wastewater,
572 Science of the Total Environment 607-608 (2017) 1213-1224.
573 https://doi.org/10.1016/j.scitotenv.2017.07.085.

574 Ahile, U.J., Wuana, R.A., Itodo, U., Sha'Ato, R., Dantas, R.F., A review on the use of
575 chelating agents as an alternative to promote photo-Fenton at neutral pH: Current trends,
576 knowledge gap and future studies, Science of the Total Environment 710 (2020) 134872.
577 https://doi.org/10.1016/j.scitotenv.2019.134872.

578 Ayers, R.S., Westcot, W., Water Quality for Agriculture; Food and Agriculture
579 Organization of the United Nations: Rome, Italy, 1985.

580 Bunting, S.Y., Lapworth, D.J., Crane, E.J., Grima-Olmedo, J., Korosa, A., Kuczynska,
581 N., Mali, A., Rosenqvist, L., van Vliet, M.E., Togola, A., López, B., Emerging organic
582 compounds in European groundwater, Environmental Pollution 269 (2021) 115945.
583 https://doi.org/10.1016/j.envpol.2020.115945.

584 Bustos, N., Cruz-Alcalde, A., Iriel, A., Fernández Cirelli, A., Sans, C., Sunlight and UVC-
585 254 irradiation induced photodegradation of organophosphorus pesticide dichlorvos in
586 aqueous matrices, Science of the Total Environment 649 (2019) 592-600.
587 https://doi.org/10.1016/j.scitotenv.2018.08.254.

588 Carra, I., Pérez Sánchez, J.A., Malato, S., Autin, O., Jefferson, B., Jarvis, P., Application
589 of high intensity UVC-LED for the removal of acetamiprid with the photo-Fenton
590 process, Chemical Engineering Journal 264 (2015) 690-696.
591 https://doi.org/10.1016/j.cej.2014.11.142.

592 Chen, L., Fu, W., Tan, Y., Zhang, X., Emerging organic contaminants and odorous
593 compounds in secondary effluent wastewater: Identification and advanced treatment,
594 Journal of Hazardous Materials 408 (2021) 124817.
595 https://doi.org/10.1016/j.jhazmat.2020.124817.

596 Ciésla, P., Kocot, P., Mytych, P., Stasika, Z., Homogeneous photocatalysis by transition
597 metal complexes in the environment, Journal of Molecular Catalysis A: Chemical 224
598 (2004) 17-33. https://doi.org/10.1016/j.molcata.2004.08.043.

599 Clarizia, L., Russo, D., Di Somma, I., Marotta, R., Andreozzi, R., Homogeneous photo-
600 Fenton processes at near neutral pH: A review, Applied Catalysis B: Environmental 209
601 (2017) 358-371. https://doi.org/10.1016/j.apcatb.2017.03.011.

602 Cruz-Alcalde, A., Sans, C., Esplugas, S., Priority pesticides abatement by advanced
603 oxidation water technologies: The case of acetamiprid removal by ozonation, Science of
604 the Total Environment 599-600 (2017) 1454-1461.
605 https://doi.org/10.1016/j.scitotenv.2017.05.065.

606 De la Cruz, N., Romero, V., Dantas, R.F., Marco, P., Bayarri, B., Giménez, J., Esplugas,
607 S., O-Nitrobenzaldehyde actinometry in the presence of suspended TiO_2 for
608 photocatalytic reactors, Catalysis Today 209 (2013) 209–214.
609 https://doi.org/10.1016/j.cattod.2012.08.035.

610 De la Obra, I., Ponce-Robles, L., Miralles-Cuevas, S., Oller, I., Malato, S., Sánchez Pérez,
611 J.A., Microcontaminant removal in secondary effluents by solar photo-Fenton at
612 circumneutral pH in raceway pond reactors, Catalysis Today 287 (2017) 10–14.
613 https://doi.org/10.1016/j.cattod.2016.12.028.

614 Dojindo Molecular Technologies, Inc, Table of Stability Constants, (2020).
615 https://www.dojindo.eu.com/images/Product%20Photo/Chelate_Table_of_Stability_Co
616 nstants.pdf (accessed May 20, 2021).

617 European Commission, Regulation (EC) No 2003/2003 of the European Parliament and
618 of the Council of 13 October 2003 relating to fertilizers, Official Journal of the European
619 Communities.

620 European Commission, Regulation 2020/741/EU of the European Parliament and of the
621 Council of 25 May of 2020 on minimum requirements for water reuse, Official Journal
622 of the European Union, 177 (2020) 32-55.

623 Food and Agriculture Organization of the United Nations. (2021). Land & Water: Water
624 scarcity. Consulted at: http://www.fao.org/land-water/world-water-day-2021/water-
625 scarcity/en/.

626 Golovko, O., Örn, S., Sörengard, M., Friedberg, K., Nassazi, W., Lai, F.Y., Ahrens, L.,
627 Occurrence and removal of chemicals of emerging concern in wastewater treatment

628 plants and their impact on receiving water systems, Science of the Total Environment 754
629 (2021) 142122.

630 Graça, C.A.L., Correia de Velosa, A., Teixeira, A.C. S.C., Role of Fe(III)-carboxylates
631 in AMZ photodegradation: A response surface study based on Doehlert experimental
632 design, Chemosphere 184 (2017) 981-991.
633 https://doi.org/10.1016/j.chemosphere.2017.06.013.

634 Guidelines for Water Reuse 600/R-12/618; Environmental Protection Agency:
635 Washington, DC, USA, 2012.

636 Huang, W., Brigante, M., Wu, F., Hanna, F., Mailhot, F., Development of a new
637 homogeneous photo-Fenton process using Fe(III)-EDDS complexes, Journal of
638 Photochemistry and Photobiology A: Chemistry 239 (2012) 17-23.
639 https://doi.org/10.1016/j.jphotochem.2012.04.018.

640 Huang, W., Brigante, M., Wu, F., Mousty, C., Hanna, K., Mailhot, G., Assessment of the
641 Fe(III)−EDDS Complex in Fenton-Like Processes: From the Radical Formation to the
642 Degradation of Bisphenol A, Environmental Science & Technology 47 (4) (2013) 1952-
643 1959. https://doi.org/10.1021/es304502y.

644 Huber, M.M., Canonica, S., Park, G.Y., Von Gunten, U., Oxidation of pharmaceuticals
645 during ozonation and advanced oxidation processes, Environmental Science and
646 Technology 37 (2003) 1016–1024. https://doi.org/10.1021/es025896h.

647 Li, J., Mailhot, G., Wu, F., Deng, N., Photochemical efficiency of Fe(III)-EDDS complex:
648 •OH radical production and 17-estradiol degradation, Journal of Photochemistry and
649 Photobiology A: Chemistry 212 (2010) 1-7.
650 https://doi.org/10.1016/j.jphotochem.2010.03.001.

651 Luo, H., Zeng, Y., He, D., Pan, X., Application of iron-based materials in heterogeneous
652 advanced oxidation processes for wastewater treatment: a review, Chemical Engineering
653 Journal 407 (2021) 127191. https://doi.org/10.1016/j.cej.2020.127191.

654 Luo, Y., Guo, W., Ngo, H.H., Nghiem, L.D., Hai, F.I., Zhang, J., Liang, S., A review on
655 the occurrence of micropollutants in the aquatic environment and their fate and removal
656 during wastewater treatment, Science of the Total Environment 473–474 (2014) 619–
657 641. https://doi.org/10.1016/j.scitotenv.2013.12.065.

658 López, N., Plaza, S., Afkhami, A., Marco, P., Giménez, J., Treatment of diphenhydramine
659 with different AOPs including photo-Fenton at neutral pH, Chemical Engineering Journal
660 318 (2017) 112-120. https://doi.org/10.1016/j.cej.2016.05.127.

661 López-Vinent, N., Cruz-Alcalde, A., Gutiérrez, C., Marco, P., Giménez, J., Esplugas, S.,
662 Micropollutant removal in WW by photo-Fenton (circumneutral and acid pH) with BLB
663 and LED lamps, Chemical Engineering Journal 379 (2020a) 122416.
664 https://doi.org/10.1016/j.cej.2019.122416.

665 López-Vinent, N., Cruz-Alcalde, A., Malvestiti, J.A., Marco, P., Giménez, J., Esplugas,
666 S., Organic fertilizer as a chelating agent in photo-Fenton at neutral pH with LEDs for
667 agricultural wastewater reuse: Micropollutant abatement and bacterial inactivation,
668 Chemical Engineering Journal 388 (2020b) 124246.
669 https://doi.org/10.1016/j.cej.2020.124246.

670 López-Vinent, N., Cruz-Alcalde, A., Giménez, J., Esplugas, Sans, C., Improvement of
671 the photo-Fenton process at natural condition of pH using organic fertilizers mixtures:
672 potential application to agricultural reuse of wastewater, Applied Catalysis B:
673 Environmental, 290 (2021) 120066. https://doi.org/10.1016/j.apcatb.2021.120066.

674 Martell, A.E., Motekaitis, R.J., Chen, D., Hancock, R.D., McManus, D., Selection of new
675 Fe(III)/Fe(II) chelating agents as catalysts for the oxidation of hydrogen sulphide to sulfur
676 by air, Canadian Journal of Chemistry 74 (1996) 1872-1879.

677 Miralles-Cuevas, S., Oller, I., Sánchez Pérez, J.A., Malato, S., Removal of
678 pharmaceuticals from MWTP effluent by nanofiltration and solar photo-Fenton using two
679 different iron complexes at neutral pH, Water Research 64 (2014) 23-31.
680 https://doi.org/10.1016/j.watres.2014.06.032.

681 Miralles-Cuevas, S., Darowna, D., Wanag, A., Mozia, S., Malato, S., Oller, I.,
682 Comparison of UV/H_2O_2, UV/$S_2O_8^{2-}$, solar/Fe(II)/H_2O_2 and solar/Fe(II)/$S_2O_8^{2-}$ at pilot
683 plant scale for the elimination of micro-contaminants in natural water, Chemical
684 Engineering Journal 310 (2017) 514–524. https://doi.org/10.1016/j.cej.2016.06.121.

685 Miralles-Cuevas, S., Oller, I., Ruíz-Delgado, A., Cabrera-Reina, A., Cornejo-Ponce, L.,
686 Malato, S., EDDS as complexing agent for enhancing solar advanced oxidation processes
687 in natural water: Effect of iron species and different oxidants, Journal of Hazardous
688 Materials 372 (2019) 129-136. https://doi.org/10.1016/j.jhazmat.2018.03.018.

689 Nahim-Granados, S., Oller, I., Malato, S., Sánchez Pérez, J.A., Polo-López, M.I.,
690 Commercial fertilizer as effective iron chelate (Fe^{3+}-EDDHA) for wastewater
691 disinfection under natural sunlight for reusing in irrigation, Applied Catalysis B:
692 Environmental 253 (2019) 286-292. https://doi.org/10.1016/j.apcatb.2019.04.041.

693 Orama, M., Hyvönen, H., Saarinen, H., Aksela, R., Complexation of [S,S] and mixed
694 stereoisomers of N,N'-ethylendiaminedisuccinic acid (EDDS) with Fe(III), Cu(II), Zn(II)
695 and Mn(II) ions in aqueous solution, Journal of the Chemical Society, Dalton
696 Transactions 24 (2002) 4644-4648. https://doi.org/10.1039/B207777A.

697 Piechowski, M., Thelen, M.A., Hoigné, J., Bühler, R.E., tert-Butanol as an OH scavenger
698 in the pulse radiolysis of oxigenated aqueous systems. Berichte der Bunsengesellschaft
699 für Physikalische Chemie 96 (1992) 1448–1454.
700 https://doi.org/10.1002/bbpc.19920961019.

701 Pignatello, J.J., Oliveros, E., Mackay, A., Advanced Oxidation Processes for organic
702 contaminant destruction based on the Fenton reaction and related chemistry, Critical
703 Reviews in Environmental Science and Technology 36 (1) (2006) 1-84.
704 https://doi.org/10.1080/10643380500326564.

705 Pupo Nogueira, R.F., Oliveira, M.C., Paterlini, W.C., Simple and fast spectrophotometric
706 determination of H_2O_2 in photo-Fenton reactions using metavanadate, Talanta 66 (2005)
707 86-89. https://doi.org/10.1016/j.talanta.2004.10.001.

708 Rodríguez-Chueca, J., Ormad, M.P., Mosteo, R., Ovelleiro, J.L., Kinetic modelling of
709 *Escherichia coli* and *Enterococcus spp*. Inactivation in wastewater treatment by photo-
710 Fenton and H_2O_2 UV-vis processes, Chemical Engineering Science 138 (2015) 730-740.
711 https://doi.org/10.1016/j.ces.2015.08.051.

712 Romero Olarte, R.V., Degradation of metoprolol by means of advanced oxidation
713 processes (Doctoral Thesis). University of Barcelona, Spain, 2015.

714 Schenkeveld, W., Temminghoff, E., The effectiveness of FeEDDHA chelates in mending
715 and preventing iron chlorosis in soil-grown soybean plants, in: H.A. El-Shemy (Ed.),
716 Soybean Physiology and Biochemistry, InTech, Rijeka, Croatia, 2011, pp 83-108.
717 https://doi.org/10.5772/21118.

718 Serra-Clusellas, A., De Angelis, L., Lin, C.H., Vo, P., Bayati, M., Sumner, L., Lei, Z.,
719 Amaral, N.B., Bertini, L.M., Mazza, J., Pizzio, L.R., Stripeikis, J.D., Rengifo-Herrera,
720 J.A., Fidalgo de Cortalezzi, M.M., Abatement of 2,4-D by H_2O_2 solar photolysis and solar

721 photo-Fenton-like process with minute Fe(III) concentrations, Water Research 144
722 (2018) 572-580. https://doi.org/10.1016/j.watres.2018.07.072.

723 Shen, J., Griffiths, P.T., Campbell, S. J., Utinger, B., Kalberer, M., Paulson, S.E., Ascorbate
724 oxidation by iron, cooper and reactive oxygen species: review, model development, and
725 derivation of key rate constants, Scientific Reports 11 (2021) 7417.
726 https://doi.org/10.1038/s41598-021-86477-8.

727 Sierra, M.A., Gómez-Gallego, M., Alcázar, R., Lucena, J.J., Yunta, F., García-Marco, S.,
728 Effect of the tether on the Mg(II), Ca(II), Cu(II) and Fe(II) stability constants and pM
729 values of chelating agents related to EDDHA, Dalton Transactions 21 (2004) 3741-3747.
730 https://doi.org/10.1039/B408730E.

731 Stasicka, Z., Chapter 7-Transition metal complexes as solar photocatalysts in the
732 environment: a short review of recent development, in: van Eldik, Rudi, Stochel, Grazyna
733 (Ed.), Advances in Inorganic Chemistry, 63, 2011, Academic Press, pp. 291e343.

734 Wu, Y., Passananti, M., Brigante, M., Dong, W., Mailhot, G., Fe(III)–EDDS complex in
735 Fenton and photo-Fenton processes: from the radical formation to the degradation of a
736 target compound, Environmental Science & Pollution Research 21 (1) (2014) 12154-
737 12162. https://doi.org/10.1007/s11356-014-2945-1.

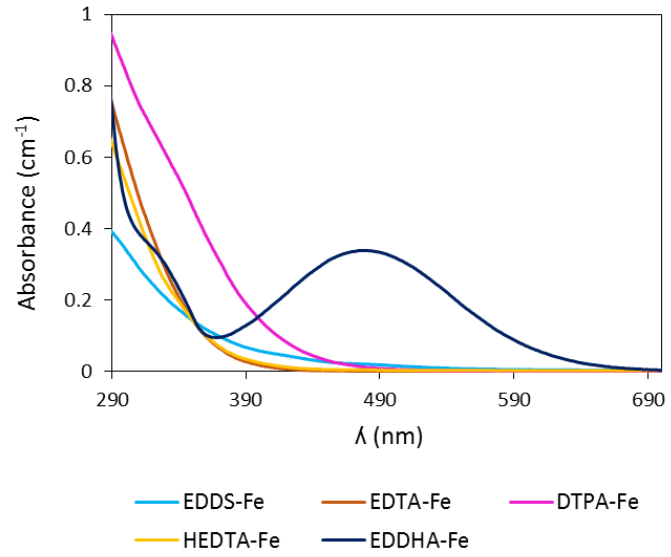

Figure 1. UV-Vis absorption spectrum of five iron chelates (EDDS-Fe, EDTA-Fe, DTPA-Fe, HEDTA-Fe and EDDHA-Fe) at 5 mg L^{-1} of iron.

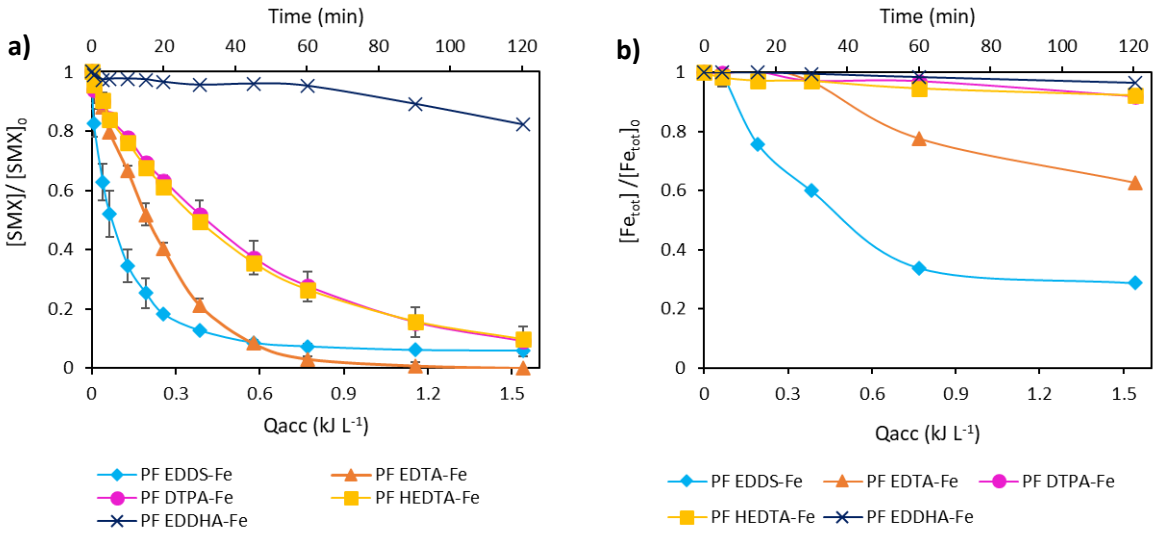

Figure 2. a) SMX abatement and b) evolution of total dissolved iron plotted as a function of the accumulated energy for photo-Fenton experiments with five different iron chelates at pH = 7.5. The pH during entire experiments was kept constant at 7.5 ± 0.2. $[SMX]_0 = 1$ mg L^{-1}; $[Fe]_0 = 5$ mg L^{-1}; $[H_2O_2]_0 = 50$ mg L^{-1}.

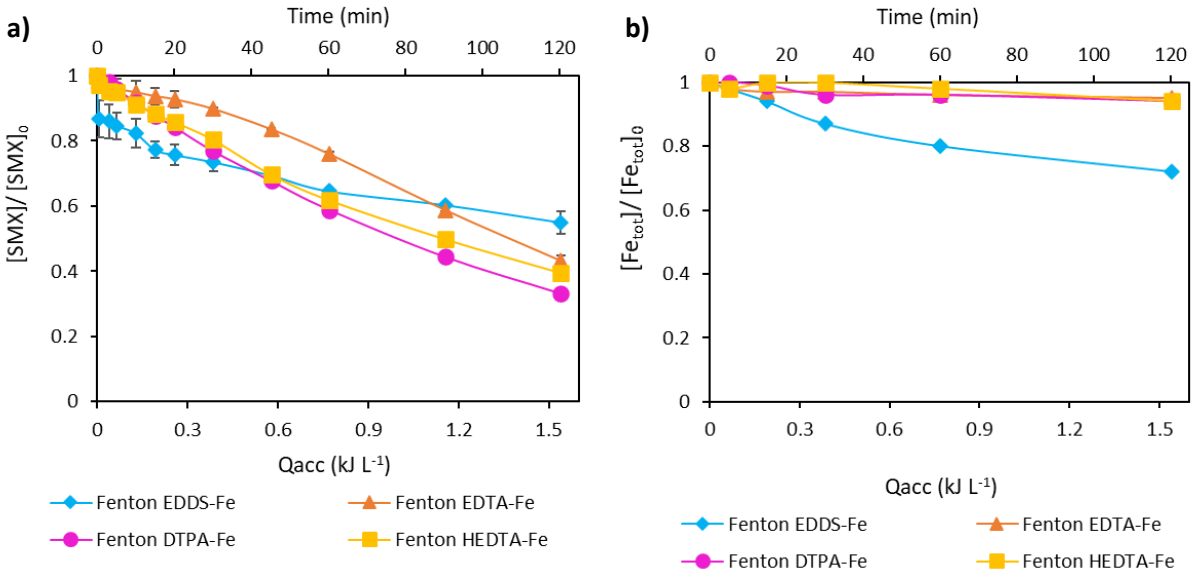

Figure 3. a) SMX abatement and b) evolution of total dissolved iron plotted as a function of the accumulated energy for Fenton experiments with four different iron chelates at pH = 7.5. The pH during entire experiments was kept constant at 7.5 ± 0.2. [$[SMX]_0 = 1$ mg L^{-1}; $[Fe]_0 = 5$ mg L^{-1}; $[H_2O_2]_0 = 50$ mg L^{-1}.

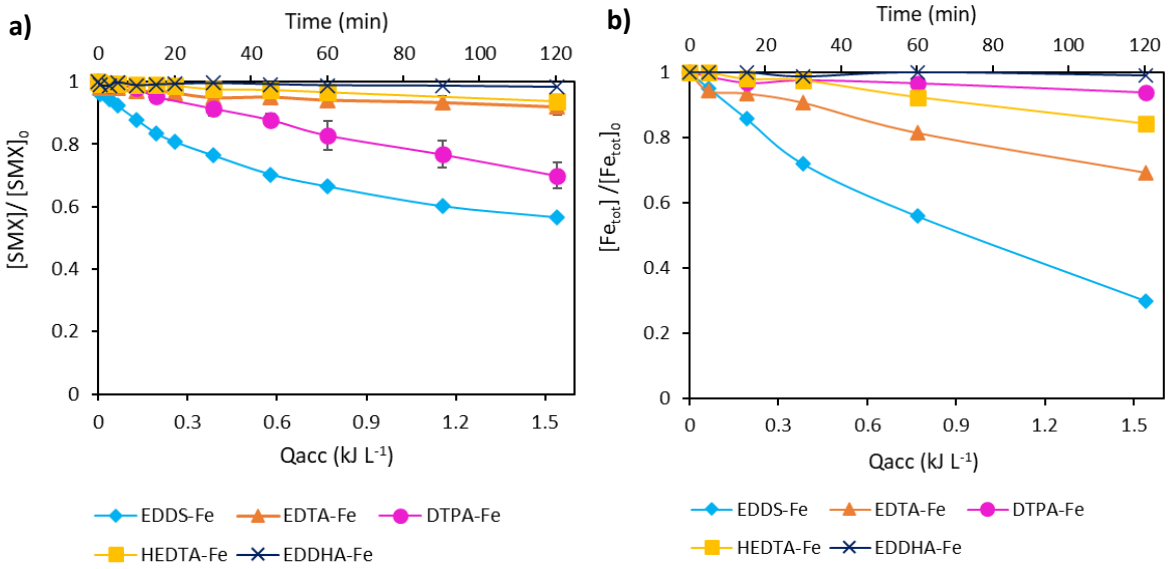

Figure 4. a) SMX abatement and b) evolution of total dissolved iron plotted as a function of the accumulated energy for irradiation experiments without H_2O_2 for five different iron chelates at pH = 7.5. The pH during entire experiments was kept constant at 7.5 ± 0.2. $[SMX]_0 = 1$ mg L^{-1}; $[Fe]_0 = 5$ mg L^{-1}.

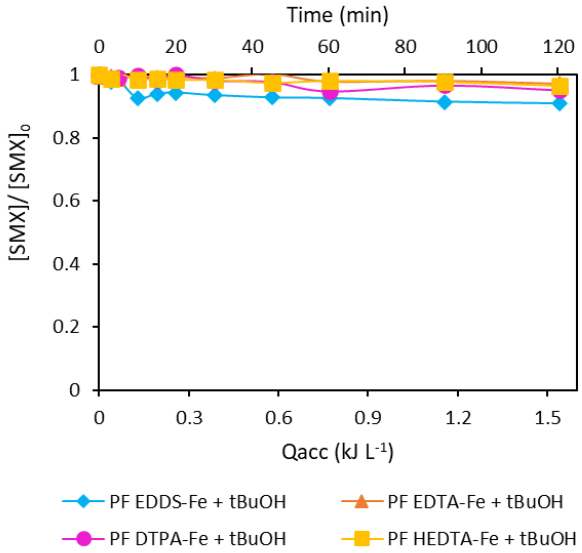

Figure 5. SMX degradation as a function of the accumulated energy for photo-Fenton experiments with tBuOH for four different iron chelates at pH=7.5. The pH during entire experiments was kept constant at 7.5 ± 0.2. $[SMX]_0$ = 1 mg L^{-1}; $[Fe]_0$ = 5 mg L^{-1}; $[H_2O_2]$ = 50 mg L^{-1}; [tBuOH] = 25 mM.

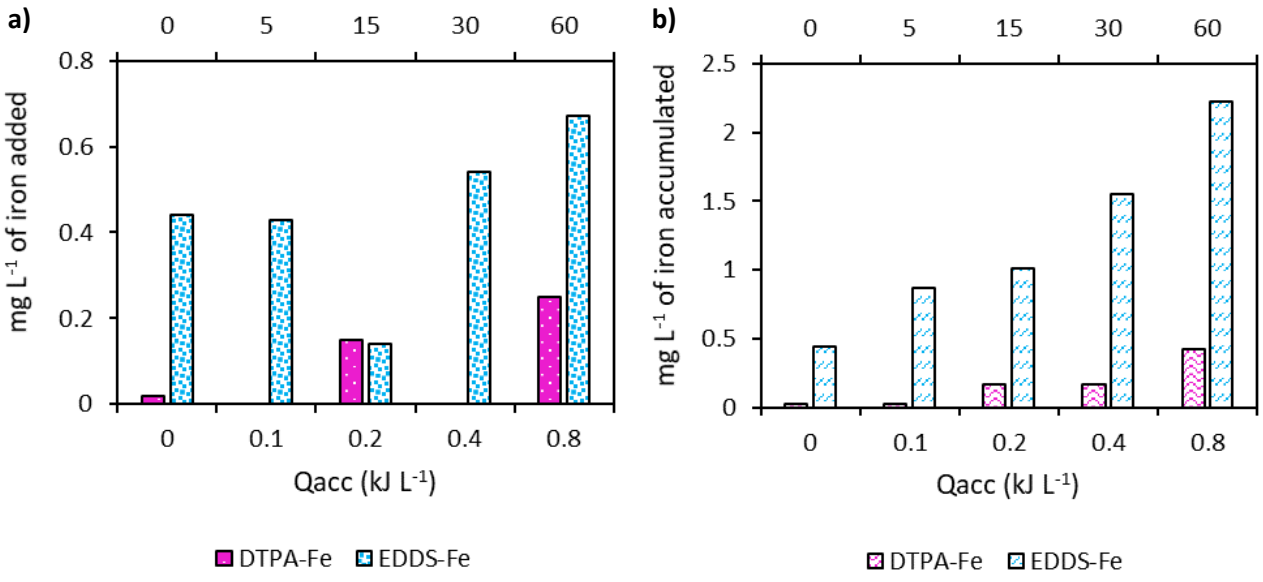

Figure 6. a) Iron dosification b) accumulated iron as a function of the accumulated energy in photo-Fenton experiments without chelating agents following the iron precipitation curves of photo-Fenton using EDDS-Fe and DPTA-Fe. pH =7.5. The pH during entire experiments was kept constant at 7.5 ± 0.2. $[SMX]_0$ = 1 mg L^{-1}; $[H_2O_2]$ = 50 mg L^{-1}.

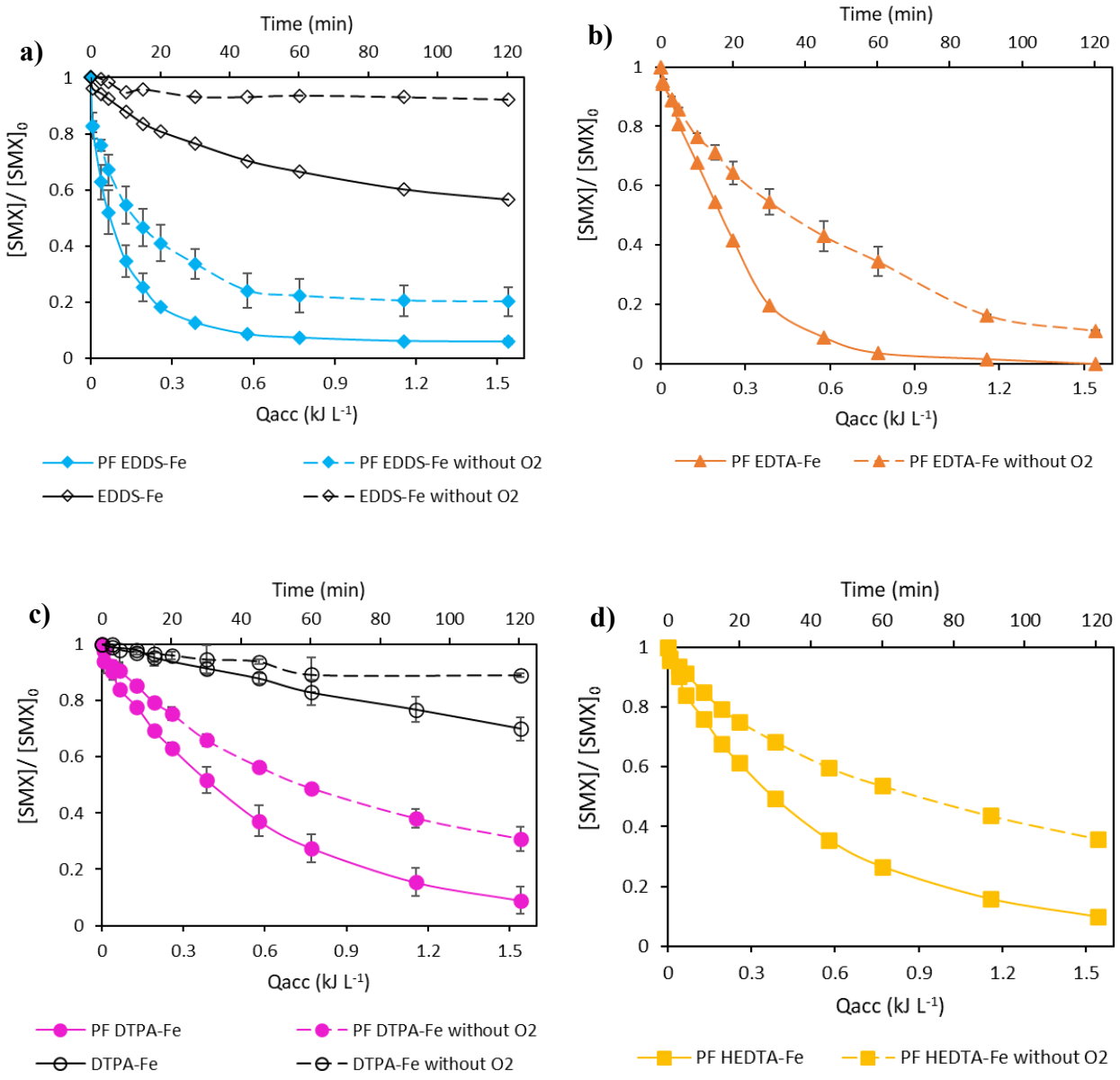

Figure 7. Photo-Fenton experiments without dissolved O_2 (continuously bubbling N_2) for a) EDDS-Fe, b) EDTA-Fe, c) DTPA-Fe and d) HEDTA-Fe as a function of the accumulated energy. Opened symbols corresponds to irradiation experiments without H_2O_2 and closed symbols refers to photo-Fenton experiments. pH =7.5. The pH during entire experiments was kept constant at 7.5 ± 0.2. $[SMX]_0 = 1$ mg L^{-1}; $[H_2O_2] = 50$ mg L^{-1}.